

## Autonomous Formation Flying Sensor for the StarLight Mission

### Authors:

**\*\* MiMi Aung, JPL, [Mimi.A.Gudim@jpl.nasa.gov](mailto:Mimi.A.Gudim@jpl.nasa.gov), FAX: (818)393-4965**  
Lawrence E. Young, JPL, [Lawrence.E.Young@jpl.nasa.gov](mailto:Lawrence.E.Young@jpl.nasa.gov), FAX: (818)393-5115  
Jeffrey Y. Tien, JPL, [Jeffrey.Y.Tien@jpl.nasa.gov](mailto:Jeffrey.Y.Tien@jpl.nasa.gov), FAX: (818)393-5115  
Jeffrey Srinivasan, JPL, [Jeffrey.Srinivasan@jpl.nasa.gov](mailto:Jeffrey.Srinivasan@jpl.nasa.gov), FAX: (818)393-5115  
George H. Purcell, JPL, [George.H.Purcell-Jr@jpl.nasa.gov](mailto:George.H.Purcell-Jr@jpl.nasa.gov), FAX: (818)393-4965  
Michael A. Ciminera, JPL, [Michael.A.Ciminera@jpl.nasa.gov](mailto:Michael.A.Ciminera@jpl.nasa.gov), FAX: (818)354-2825  
Yong J. Chong, JPL, [Yong.J.Chong@jpl.nasa.gov](mailto:Yong.J.Chong@jpl.nasa.gov), FAX: (818)393-5115  
Luis R. Amaro, JPL, [Luis.R.Amaro@jpl.nasa.gov](mailto:Luis.R.Amaro@jpl.nasa.gov), FAX: (818)393-0050

### \*\* Contact author

All authors are from the Jet Propulsion Laboratory, California Institute of Technology, Pasadena, California, United States of America.

### *1.0 Introduction*

The StarLight Mission, an element of NASA's Origins Program, was designed for first-time demonstration of two technologies: formation flying optical interferometry between spacecraft and autonomous precise formation flying of an array of spacecraft to support optical interferometry.<sup>1</sup> These technologies will be applicable to future missions such as the Terrestrial Planet Finder (TPF), Planet Imager, MAXIM, and other deep space missions requiring deep space, autonomous, precise formation flying to enable a distributed instrument to operate cooperatively across multiple spacecraft. The StarLight mission is composed of two spacecraft, the Collector spacecraft and the Combiner spacecraft (see Figure 1). After initial checkout in a heliocentric, Earth-like orbit, the two spacecraft separate and begin flying in formation at separations between 30 and 1000 meters, without real-time intervention from ground-based Mission Operations. Operation of the optical interferometer requires alignment of the relative optical path delay to 20 arc-seconds and nano-meter levels of accuracy. This is achieved in multiple steps, starting from a lost-in-space condition. In the first step, a radio frequency (RF) system, the Autonomous Formation Flying (AFF) Sensor, is used to enable precise formation flying with control accuracy of  $\pm 10$ cm in range and  $\pm 4$  arc-minutes in bearing angle. This accuracy is within the search range of the optical metrology system. Optical metrology first uses siderostats (steerable mirrors) to direct light from the collector to the combiner, achieving 20 arc-seconds of pointing accuracy. Next, the delay line within the interferometer aligns the optical path delay to a nano-meter level.

---

<sup>1</sup> In February 2002, StarLight mission was cancelled by NASA owing to funding unavailability. At that time, portions of StarLight technology work applicable to the Terrestrial Planet Finder (TPF) mission were adopted by the TPF technology program. The Autonomous Formation Flying (AFF) Sensor technology work was adopted. In this paper, the AFF Sensor is presented within the StarLight context. The AFF Sensor technology will be carried forward to the TPF design.

For acquisition and maintenance of a precise spacecraft formation, a relative sensor is required to provide knowledge of spacecraft separation with a maximum uncertainty of 2 cm, provide knowledge of the bearing angles of the remote spacecraft with a maximum uncertainty of a minute of arc, transmit radiometric data between spacecraft, and operate with a wide field of view. For this purpose, an RF sensor, the AFF sensor, was designed. It operates at Ka-band across a pair spacecraft as illustrated for StarLight in Figure 1.

A significant challenge lies in the simultaneous requirements for precision and a wide field of view mandating a substantial technology development effort and design of a sensor with some novel features. To retire the key technology risks, a prototype Ka-band AFF Sensor was developed to verify the basic algorithms and the complexity of the system distributed over multiple spacecraft, and to assess the end-to-end performance in the spacecraft structural environment. The design overview and results of the technology effort are presented in this paper.

Figure 1. INSERT STARLIGHT PICTURE HERE

### ***3.0 Key Features and Performance Requirements***

The AFF sensor is novel in that it performs all of the following functions:

1. It provides unprecedented accuracy in real-time range and bearing angle measurements ((2 cm, 1 arcmin) 1- $\sigma$  accuracy at spacecraft separation up to 1km in the “facing” configuration defined below).
2. It operates with a nearly 4- $\pi$  steradian field of view coverage.
3. It operates autonomously:
  - a. No real-time ground-based interaction
  - b. Self-contained instrument: Transmit, receive and data communication HW/SW between multiple spacecraft
  - c. Applicable to deep space missions (the Earth-based GPS system is not used.)
4. It generates estimates of range and bearing angle for use in real-time by the formation flying control system.

AFF sensor range and bearing angle estimation requirements are as follows. The most stringent requirements are when the spacecraft are directly facing each other in the interferometric observation mode. This is when the stellar interferometer will acquire the optical signals. The requirements are gradually relaxed for larger off-pointing angles where the AFF sensor is used to steer the formation to the required geometry. As such, the requirements are specified for three regions:

**Facing:** angle  $\alpha$  between lines of sight and normal to front side of spacecraft  $\leq 2^\circ$ , both spacecraft

**Nearly facing:**  $2^\circ < \alpha \leq 45^\circ$  for more mis-pointed spacecraft.

**Not facing:**  $45^\circ < \alpha$  for even more mispointed spacecraft.

	Ground calibration and internal measurements			With phase-calibration by spacecraft rotation			After bias-calibration with laser metrology		
	Facing	Nearly Facing	Not Facing	Facing	Nearly Facing	Not Facing	Facing	Nearly Facing	Not Facing
<b>Range (cm)</b>	2	2-30	160	2	2-30	160	2	2-30	160
<b>Range Rate (mm/s)</b>	1	1	none	1	1	none	1	1	none
<b>Bearing Angles (°)</b>	10	10-900	5400	5	5-600	5400	1	1-600	5400
<b>Bearing Rate (°/s)</b>	10	20	none	10	20	none	10	20	none
<b>Acquisition Time (s)</b>	300	300	none	300	300	none	300	300	none

Table 1: Requirements for AFF sensor performance

### 3.0 Design Overview

The AFF sensor is a distributed RF sensor that operates at Ka-band. It is a self-contained system with transmitters and receivers for both radiometrics and data transfer on both spacecraft. It consists of virtually identical hardware and software on each spacecraft. Each spacecraft will have 2 transmitting antennas and 4 receiving antennas:

- 1 transmitting antenna and 3 receiving antennas on the facing or front side
- 1 transmitting antenna and 1 receiving antenna on the back side

The antennas on the facing side are to align the spacecraft to the required level. The antennas on the back are to assist the spacecraft in finding each other in the event they get turned around. This configuration will give near-global coverage.

The two halves of the sensor transmit to and receive from the other spacecraft in full-duplex. The signal structure is similar to that used by the GPS:

$$S(t) = A P(t) D(t) \text{Cos}(2\pi ft + \phi)$$

where

$A$  = signal amplitude

$P(t)$  = ranging code

$D(t)$  = telemetry modulation

$f$  = Ka-band carrier frequency

$\phi$  = carrier phase due to range, clock offsets, etc.

The relative range between the two spacecraft is determined from the delay tracked with the ranging codes. The bearing angles (azimuth, elevation) are determined from the differential carrier phases. Telemetry is modulated across the duplex to enable the instruments on each spacecraft to compute range and bearing estimates.

The transmitter and receivers on two halves of the sensor can transmit and receive simultaneously, or operate in a time-division duplexing (TDD) mode, where on a given spacecraft, the transmission is turned on and off in cycles, and the receivers process signals only when the transmission is off. Multiple versions of TDD scheme exist, some requiring time-synchronization across spacecraft while other do not. For StarLight, the latter can be employed.

### *3.1 Building Blocks of the AFF Sensor*

The AFF Sensor is composed of Ka-band antennas, Ka-band transceivers, frequency and timing subsystems, and digital baseband processors. For optimal RF performance of the sensor within the spacecraft structural environment, a Ka-band antenna was designed with goal to maximize field of view and minimize back-lobe energy. In the transceivers and the frequency and timing subsystem, a complex frequency scheme was designed to enable the acquisition and calibration of the sensor distributed over multiple spacecraft. The digital signal processor performs the radiometric processing.

The sensor design and performance have strong inter-play with the spacecraft and interferometer designs. They are inter-dependent in terms of accommodations, fields-of-view, stray light, radio frequency interference, thermal stability, electrical stability and mechanical stability.

### *3.2 Acquisition*

After launch and separation of the two spacecraft, the AFF sensors need to acquire the RF carriers, codes, and data. A proprietary acquisition scheme has been developed to minimize the acquisition time, and to allow robust acquisition under low-signal conditions when the antennas are not aligned.

### *3.3 Calibration*

After signal acquisition across the full duplex, the sensor needs to be calibrated in the following manner.

#### *3.3.1 Antenna Pattern Calibration with spacecraft rotations*

The antennas phase patterns will be calibrated prior to launch. However, due to deformations expected at launch, we expect to apply in-flight calibration procedures to achieve the high-level of accuracy required by the bearing angle requirement. In-orbit calibrations must be performed. The relative phases between the pairs of antennas on a spacecraft are calibrated through observation of the phase changes while maneuvering the spacecraft through bearing angle changes known from each spacecraft's star camera.

#### *3.3.2 Continuous Self-Calibration for Instrumental Variations*

Spacecraft thermal, electrical and mechanical variations can introduce instrumental variations which can significantly degrade the sensor performance. Therefore, self-calibration algorithms are employed for continuous internal calibration.

### *3.3.3 Residual Bias Calibration with Metrology System*

Residual biases after above calibrations are calibrated by comparing the AFF sensor estimates to the finer accuracy metrology system estimates.

## **4.0 Key Technical Challenges**

The key technical challenges for the AFF sensor to meet the tight performance requirements while operating with a wide field of view in an autonomous environment include:

- Adequate RF performance within the spacecraft structure
- Range and bearing angle estimation in the presence of thermal, electrical and mechanical instabilities on the spacecraft
- Spacecraft accommodations to satisfy spacecraft and interferometer requirements
- Calibration of the distributed system
- Signal acquisition of the tracking signal by all receivers
- Operation as a single instrument distributed among multiple spacecraft.

### *4.1 RF performance within the spacecraft structure*

The spacecraft structure surrounding the antennas modify the effective pattern of the antenna, due to multipath and diffraction effects. Two major concerns to the sensor performance are: (1) the isolation between the transmitting antennas and the receiving antennas; and (2) deviation of the antenna patterns from the nominal pattern.

### *4.2 Thermal, electrical and mechanical instabilities on the spacecraft*

Spacecraft thermal, electrical and mechanical variations can introduce instrumental variations. For the precise levels of performance requirements, the sensor is sensitive to even the slight variations that can contribute significant degradation in performance.

### *4.3 Spacecraft Accommodations*

In a formation flying interferometer mission, the RF sensors and the optical instruments need to be accommodated and operated harmoniously. The AFF sensor operates across the same hemisphere as the metrology and starlight paths and conflicting requirements stem from the RF and the optical aspects. An example is the antenna. Ideally, the RF antennas are made of reflective materials, while the optical system requires all structures to be black to mitigate stray light. Another example is the sunshade. A sunshade is necessary for the optical interferometer to prevent stray light and for thermal protection.

For the RF sensor, the sunshade is the primary source of multipath. RF interference (RFI) with spacecraft subsystems is another area to beware. Physical accommodation of all the instruments also has to be coordinated. Overall, a careful system engineering effort is required during mission design.

#### *4.4 Calibration of the Distributed System*

In-orbit calibration of the antenna phase pattern and removal of residuals require analytical and operational coordination with the spacecraft maneuver control and metrology system, e.g. knowledge of relative maneuvers, communications latency.

#### *4.5 Acquisition of the Spacecraft Formation*

Immediately after launch, the two spacecraft sun-point themselves into the sunshaded positions. After that, the formation flying system needs to control the formation to an accuracy of  $\pm 10$ cm in range and  $\pm 4$  arc-minutes in bearing angle. A complex acquisition design is required for formation control and sensing systems.

#### *4.5 Synchronization of the Distributed System*

Given the fact that the sensor is distributed across multiple spacecraft, the following issues need to be addressed carefully: Time synchronization, independent reference frequency bases, multiple frequency schemes, inter-spacecraft communications, fault-protection and recovery for cases of partial failures in the multiple-spacecraft formation.

### **5.0 Technology Development and Results**

In leading technology risk items were investigated in order to assess the feasibility of the AFF sensor for StarLight formation flying. A prototype AFF sensor was developed and the sensor was evaluated in three avenues. The RF antenna performance was addressed in the antenna testbeds. The sensor scheme and the algorithm performance were tested in the AFF Sensor prototype testbed. The end-to-end functionality test was performed outdoors across a 1200 foot range. Through these tests, many of the technical concerns have been understood and retired, while other concerns provided insight leading to modification of the baseline design.

The leading technical concerns addressed were:

- (1) RF antenna performance – evaluated in the antenna testbeds
  - a. Isolation between transmitting and receiving antennas
  - b. Antenna pattern degradation due to multipath and diffraction effects
- (2) Basic algorithms and calibration schemes in a multiple-spacecraft environment (i.e. with separate frequency references on each spacecraft) – evaluated in the prototype testbed
  - a. Basic signal processing algorithms
  - b. Continuous self-calibration algorithm
  - c. Algorithm for carrier-aided smoothing of the range observable

- d. Asynchronous TDD scheme
- e. End-to-end complex Ka-band scheme

(3) End-to-end functional test performed outdoors across a 1200-foot range.

A comprehensive error budget analysis was performed, and results from the testbeds were evaluated against the error budget allocations. The descriptions of the testbeds, results and a summary of the technology assessment are presented in this section.

### 5.1 RF antenna performance – evaluated in the antenna testbeds

The performance of the Ka-band antennas within the StarLight spacecraft structural environment was evaluated in the following antenna testbeds. The antennas were prototyped and physical models of the antenna mounting plate and the spacecraft sunshades (for both the Combiner and the Collector spacecraft) were constructed. Then, the performance of each antenna was assessed within the structurally modeled environment.

#### 5.1.1 Isolation between Transmitting and Receiving Antennas

To evaluate the isolation between the transmitting and receiving antennas, the antennas and the structural models were set up as shown in **Figure 2**. The transmitting antenna and the adjacent receiving antennas were pointed towards the sky. While the transmitting antenna transmitted, the signals received at the receiving antennas were measured. Isolation of each receiving antenna was defined as the ratio of the received signal power to the transmitted power. Measurements were made with and without the sunshade models attached. Results are significant.

1. The measured isolation matches exactly the predicted path loss through air per Friis's equation. This is a significant, positive result that indicates that there are no surface effects on the mounting plate. This is further supported by the fact that the isolation level remained unchanged when the plate was removed and when multi-layer insulation (MLI) was laid on the plate. Insensitivity to MLI is positive as MLI may be necessary for thermal control.
2. The isolation between the transmitting and receiving antennas were degraded by the multipath and diffraction effects from the sunshade. The degradation depended directly upon the shape of the sunshade. Without the sunshade, isolation levels varied in the range (-91 dB, -85 dB) with the change in the position of the sunshade relative to the antenna. With the Combiner sunshade, the range spanned over (-80 dB, -73 dB). With the Collector sunshade which has the sharper slope away from the antennas, isolation ranged over (-86 dB, -80 dB). The sharper the angle of the sunshade away from the antennas, the less was the level of degradation to the isolation. Insufficient isolation deemed the Time-Division Duplexing to be necessary to prevent self-jamming.
3. Repeatability of the isolation levels when the separation between the antennas and the sunshades was varied was poor. This is due to the fact that the uncertainty in

mechanical positioning is comparable to the short wavelengths at Ka-band. This fact must be taken into account when considering using the transmitted leakage signal as a part of the self-calibration scheme, as biases can be introduced easily by pre- and post-launch shifts in the sunshade and thermal variations. This uncertainty reinforces the use of a TDD scheme, where a self-calibration signal on a controlled path will not be varied during reception.

### *5.1.2 Effect of the Multipath and Diffraction Effects upon the Antenna Pattern*

For evaluating the effect of the multipath and diffraction upon the antenna pattern, tests were set up in an anechoic chamber as shown in Figure 3. The transmitting and receiving antennas were mounted on the model of the mounting plate, and patterns were cut with and without the sunshade models attached. A pair of patterns, the first without the sunshade, and the other with a sunshade are shown in Figure 4. These results show that range and bearing error contribution from the antenna pattern degradation are not negligible.

To evaluate the impact of the antenna pattern deviations on the RF performance, the worst-case deviation from the ideal pattern was measured and its contribution to the error in estimation of the range and bearing angle estimates was evaluated. The error contribution was compared to the error budget allocation. The results showed that within the overall error budget, the deviations due to multipath and diffraction effects are well within the error allocation. In the “facing” configuration, the sensor can meet the (2 cm, 1 arcmin) requirement in range and bearing angle estimation. In the “nearly-facing” and “not facing configurations”, the deviations still satisfied the looser requirements for those regions. This shows that the performance requirements can be met in the StarLight configuration.

### *5.2 Basic algorithms and calibration schemes in a multiple-spacecraft environment – evaluated in the prototype testbed*

To verify the basic algorithms and calibration schemes in a multiple-spacecraft environment, a prototype sensor testbed was developed. The testbed is shown in Figure 5. It is composed of two halves, each side representing a spacecraft. Each half is composed of the Ka-band modules and a digital baseband processor. The waveguides connecting the two halves represent the space-loss. The testbed operates with the AFF sensor frequency scheme operating across two independent halves of the duplex. The two halves are operated from independent frequency bases. Microwave assemblies are thermally controlled for studies involving thermal variations. This prototype is fully operational. The test results are discussed below.

#### *5.2.1 Continuous Self-Calibration Scheme*

A continuous self-calibration scheme has been designed to calibrate across the duplex. This scheme has been verified on the prototype system. Results of self-calibration on the phase observable and the range observable are shown in Figure 6. It is clear from the

results that the instrumental variation on the phase and range observables are removed by the full calibration technique.

### *5.2.2 Carrier-aided Range Estimation*

The AFF sensor employs a GPS-based scheme for smoothing the range observable with the aid of knowledge of the carrier phase from the carrier tracking loop. This algorithm is successfully used in the GPS system. However, it is novel for the AFF system because unlike the GPS system where the carrier and code are transmitted from the highly stable sources onboard the GPS satellites, the AFF system generates its own transmitted signals. As such, stability of the transmitting and receiving Ka-band modules and the frequency and timing scheme have to be assessed with respect to feasibility of this algorithm. Results shown in Figure 7 show that the AFF scheme can indeed support this algorithm. Figure 7(a) shows the range observable before carrier-aided smoothing, and Figure 7(b) shows the observable after 100 seconds of smoothing. The standard deviation about the observable is reduced by the expected ratio.

### *5.2.3 Asynchronous Time-Division Duplexing (TDD)*

An asynchronous version of time-division duplexing scheme which does not require the two spacecraft to be synchronize in the duplexing has been verified on the prototype. The reduction in the signal-to-noise ratios due to duplexing matched that of the predicted.

### *5.2.4 Ka-band Frequency Scheme*

The successful prototype test results confirm that the Ka-band frequency scheme selected for StarLight will work.

### *5.3 End-to-end Functionality Test of the AFF Sensor*

An end-to-end radiated test will be performed in October 2002 to verify the end-to-end functionality of the sensor. The two halves of the sensor will radiate across the duplex over a 1200-foot valley behind JPL. The test setup is shown in Figure 9.

### *5.4 Summary of the Technology Results*

AFF sensor evaluation tests were performed in three avenues. The antenna testbeds (Figures 2 and 3) were used to verify the RF antenna performance, while the AFF Sensor prototype testbed (Figure 5) was used to verify the sensor scheme and the algorithm performance. The end-to-end functionality test completes the full assessment of the sensor. Through these tests, many of the technical concerns have been understood and retired, while other concerns provided insight leading to modification of the baseline design.

The concerns which have been retired at this time are:

- (4) algorithms for self-calibration,

- (5) algorithms for carrier-aided smoothing of the range observable;
- (6) antenna pattern degradation due to multipath and diffraction effects;
- (7) verification of the complex Ka-band scheme.

One concern that proved to be not workable leading to modification of the baseline design was the isolation between the transmitting and receiving antennas in the presence of multipath and diffraction effects. Insufficient isolation and uncontrolled variations discouraged the use of leakage signal for self-calibration and encouraged that use of time-division duplexing (TDD) to prevent self-jamming. The TDD scheme has been verified to work within the AFF Sensor scheme by tests in the prototype testbed.

## *6.0 Associated StarLight Design*

### *6.1 Spacecraft Accommodations*

For spacecraft accommodation, the spacecraft design team accommodated the AFF sensor antennas as close to the edge as possible, but still behind the sunshade, as shown in Figure 8. Figure 8(a) shows the accommodation on the Combiner spacecraft, and Figure 8(b) shows that accommodation on the Collector spacecraft. In the ideal case, the antenna plates should be mounted at edge of the sunshades with no structures in view of the antennas. In reality, Figure 8 was the optimal compromise.

The sensor will need to be calibrated with the final sunshade design. Selection of the sunshade material and geometry had not been completed. This is a technology area of challenge in satisfying the optical, RF and thermal requirements simultaneously.

### *6.2 Acquisition of Spacecraft Formation*

The control system requires the widest field of view possible from the RF sensor to minimize the search time. A trade-off has to be performed between the AFF sensor field of view (which include the antennas and the sunshade design), control system design and the associated number of spacecraft maneuvers. Further, there is a trade-off between the sensor field of view and multipath effects degrading the sensor performance, which in turn must be traded off with the control system design.

Currently, a  $\pm 70^\circ$  field of view antenna has been designed and assessed for RF performance. Further iterations of field of view versus performance is anticipated in the mission design stage.

### *6.3 Synchronization of the Distributed System*

Distributed nature of the sensor across the two spacecraft pose challenges in terms of time synchronization, fault-protections, and recovery from one or both of the halves failing temporarily. Given that the sensor is support an optical interferometer, the maximum robustness and minimum maintenance design is required. Further work is required in this area.

## **6.0 Conclusion**

At this time, the AFF sensor has been fully assessed. The leading technical challenges have been addressed through development of a prototype AFF sensor and tests in multiple testbeds for performance evaluation and end-to-end functional verification. The results show that the sensor will work with the required performance of (2cm, 1 armin) 1- $\sigma$  accuracy in range and bearing angle estimates within the StarLight mission.

These results are directly applicable to the TPF mission. For TPF and any other precision formation flying mission, it is emphasized that the sensor performance needs to be optimized through trade-off between the sensor design, spacecraft design and the optical interferometer (or any other science instruments) design for the mission. For the precision formation flying system, performance must be optimized through trading off the sensor performance, sensor field of view, spacecraft maneuvers and formation control design.

## **6.0 Further Work**

The AFF Sensor will be further assessed for integration into the TPF precision formation flying system. In particular, the following technical assessments need to be made for the TPF spacecraft configuration: multipath and diffraction effects, acquisition techniques, calibration techniques, hand-off to a finer sensor with a narrower field of view, and trade-off between sensor performance, field of view, formation flying control design, spacecraft design and the interferometer design.

Another set of future work is to investigate technologies to integrate high-bandwidth inter-spacecraft communications with the AFF sensor. This concept is motivated by the fact that the sensor already provides an inter-spacecraft link with highest performance in the "facing" configuration. For the interferometer, the highest data bandwidth requirement is required in the "facing" configuration to enable high-speed control loops for the siderostat control system.

### ***Acknowledgement***

The authors would like to acknowledge the collaboration of Ball Aerospace & Technologies Corporation, Boulder, Colorado, U.S.A., and particularly Mike Weiss, Dean Paschen and Andy Jarski, for their contributions to the AFF sensor technology activities. Their work on the mutual accommodation of the spacecraft and the AFF Sensor was crucial to the Sensor's development, and they provided the designs for the spacecraft structural models used in our testing.

### **Figures:**

Figure 1: StarLight mission (showing two spacecraft w/ RF and optical paths)

Figure 2: Test setup for antenna isolation tests

Figure 3: Test setup for the antenna pattern tests with and without sunshade mock-ups

Figure 4: Antenna pattern with and without sunshade.

Figure 5: AFF prototype system testbed

Figure 6: (a) single channel phase measurement; (b) single-differenced phase observable; (c) double-differenced (fully calibrated) phase observable; (d) single-channel delay measurement; (e) summed range observable; (f) fully calibrated range observable.

Figure 7: (a) Range observable before carrier-aided smoothing; (b) Range observable after 100 seconds of smoothing.

Figure 8: (a) AFF sensor accommodation on the Combiner s/c; (b) AFF sensor accommodation on the Collector s/c

Figure 9: Radiated test pictures



Figure 1: AFF Sensor within StarLight Mission



With no sunshade



With Collector s/c sunshade



With Combiner s/c sunshade

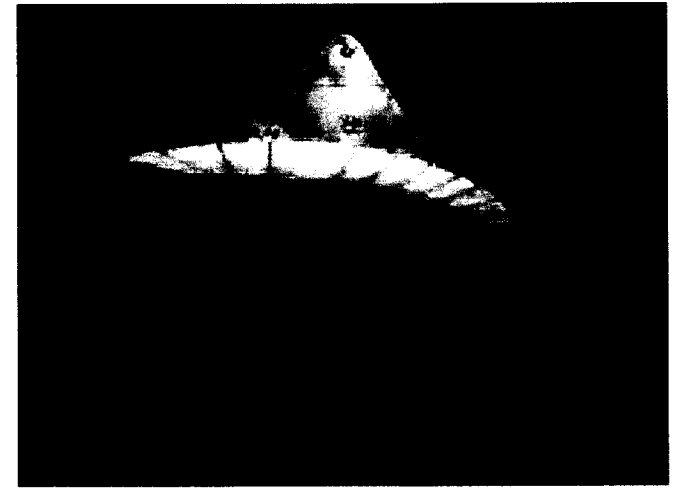
Figure 2: Test setups for the isolation between transmitting and receiving antennas



With no sunshade



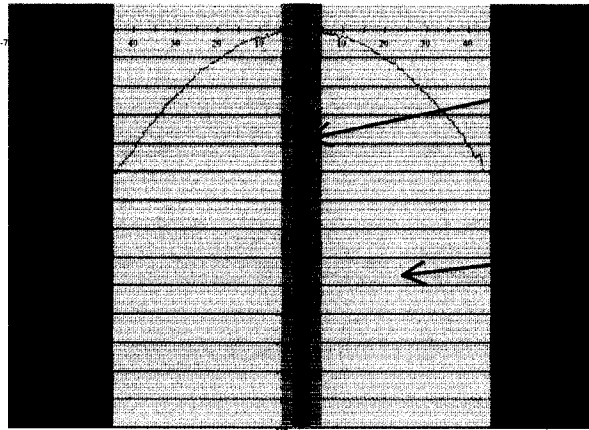
With Collector sunshade



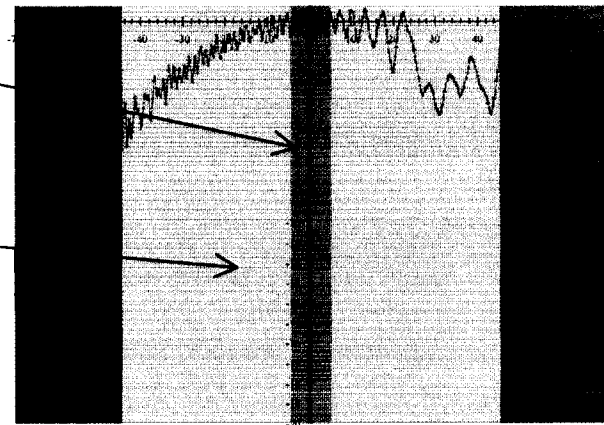
With Combiner sunshade

Figure 3: Test setups for pattern measurements with and without the sunshades

Antenna gain pattern with no sunshade



Antenna gain pattern with combiner sunshade



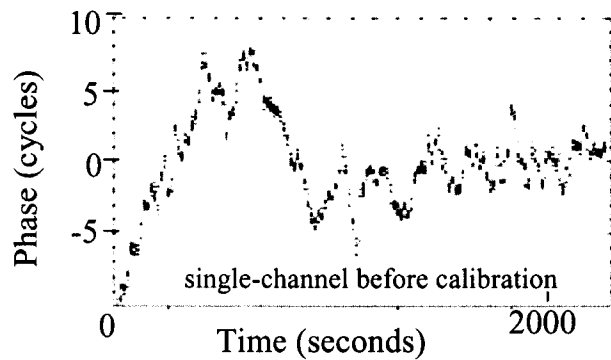
directly-facing region

nearly-facing region

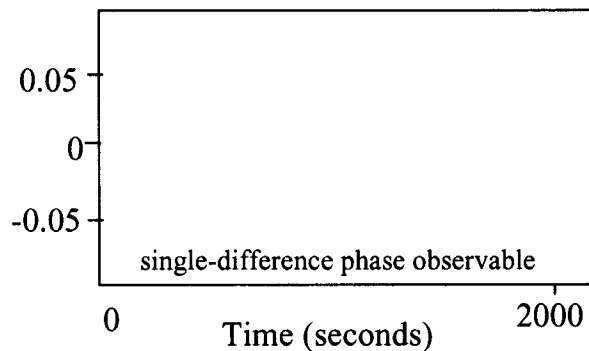
Figure 4: Antenna patterns with and without the sunshades



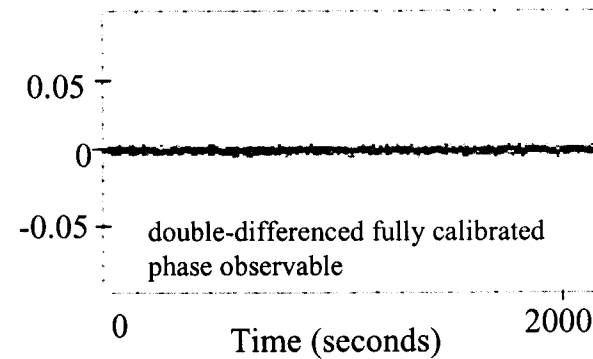
Figure 5: AFF prototype system testbed



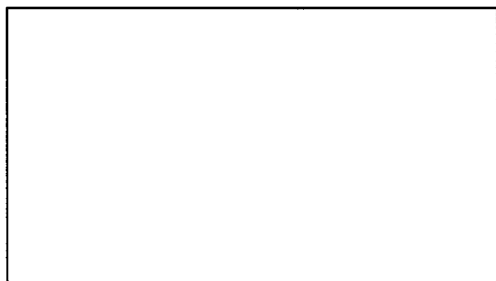
(a)



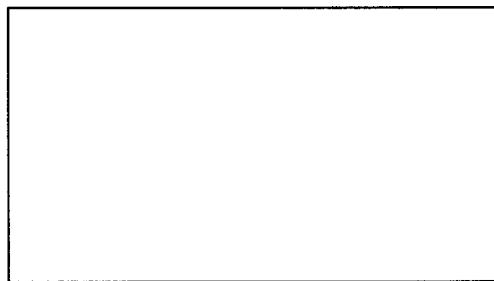
(b)



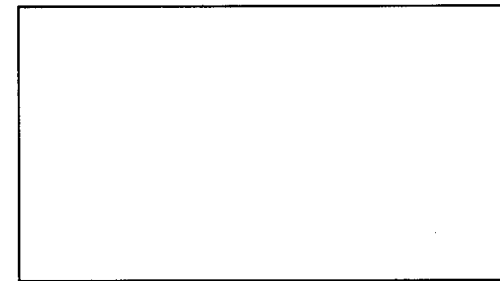
(c)



(d)



(e)



(f)

Figure 6: Continuous calibration results: (a) single channel phase measurement; (b) single-differenced phase observable; (c) double-differenced (fully calibrated) phase observable; (d) single-channel delay measurement; (e) summed range observable; (f) fully calibrated range observable.

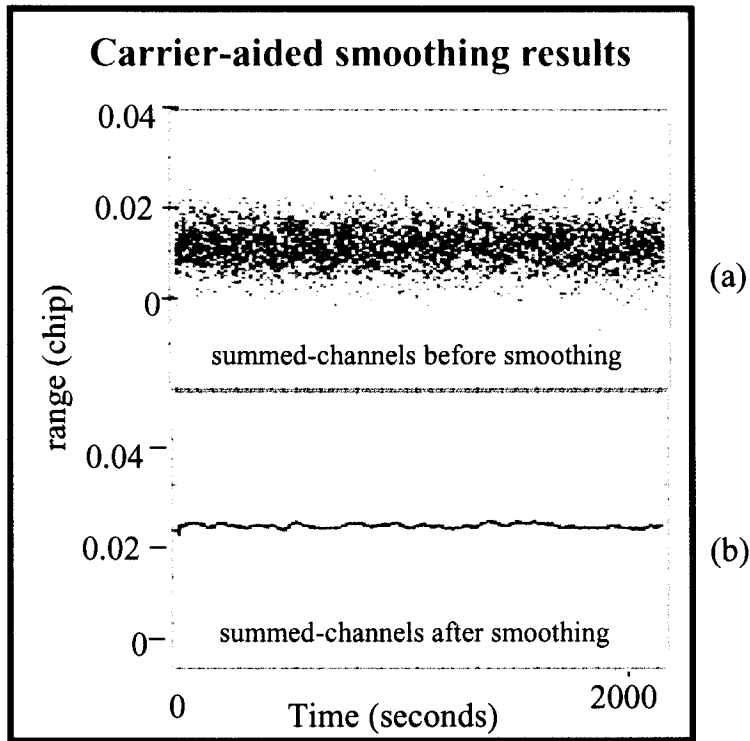


Figure 7: Results of carrier-aided smoothing on range observables: (a) Range observable before carrier-aided smoothing; (b) Range observable after 100 seconds of smoothing.

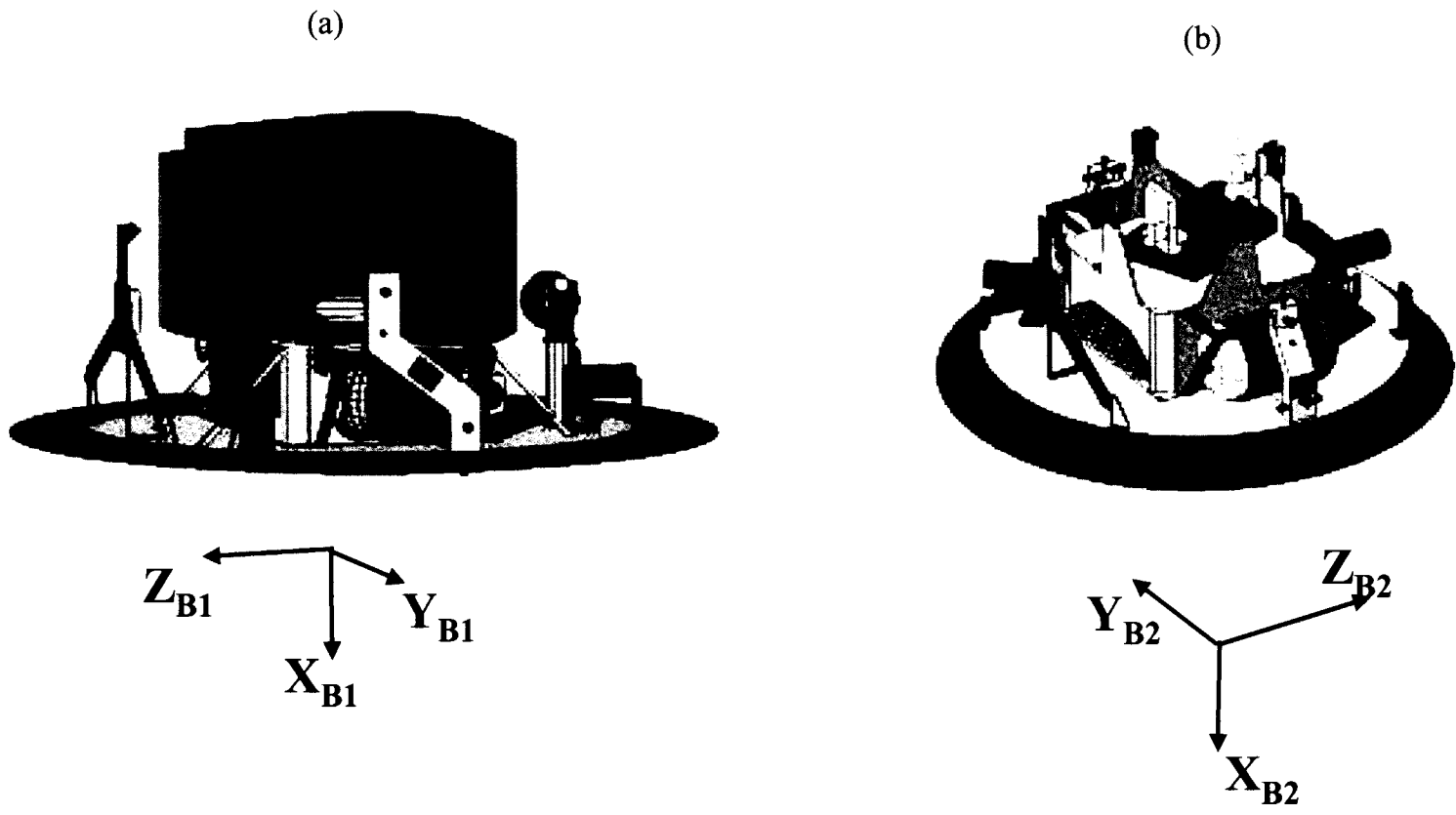


Figure 8: (a) AFF sensor accommodation on the Cominber s/c; (b) AFF sensor accommodation on the Collector s/c



Figure 9: AFF Sensor radiated test for end-to-end functional verification